# Assessment of Communication Channel Effects on Time-Domain Protection Functions Tripping Times

Eduardo P. A. Ribeiro, Felipe V. Lopes, Kleber M. Silva, Amauri G. Martins-Britto

***Abstract*—This paper investigates the effects of communication channel latency (CCHL) on time-domain line protection functions. The Alternative Transients Program (ATP) was used to simulate the monitored power system and to model both the analyzed relays and communication channels via MODELS language. By doing so, the need for extra long optical fibers for laboratory tests is overcome. To provide a reliable investigation on the CCHL effects, a time-domain relay model is firstly implemented and validated by comparing its response against an actual device. Then, the communication channel is set to properly represent practical CCHL values under different fault scenarios for transmission lines with different lengths. The obtained results show that including the CCHL effects on time-domain protection testing procedures is of utmost importance because, depending on the data propagation time through the communication channel, it may have a relevant influence in what we call here "race of protection functions".**

***Keywords*—ATP, MODELS language, communication channel latency, time-domain line protection.**

## I. Introduction

OVER the last years, time-domain-based transmission line (TL) protection relays have been released on the market. These devices do not require the phasor estimation process, so that data windowing process is no longer required. As a result, by using time-domain protection functions, high-speed fault clearance becomes feasible in critical fault scenarios, reducing the traditional tripping times to the order of a few milliseconds [1]–[4].

The above-mentioned benefits have been reflected in the gain of notoriety by time-domain protections, motivating the development of time-domain relay models to support protection studies. For instance, in [5], the impacts of an LCC-HVDC system on time-domain protective schemes applied to surrounding AC TLs are assessed using an ATP/MODELS relay model. In [6] an evaluation of a time-domain-based differential protection when applied on hybrid transmission lines is carried out, highlighting the impact of using different settings on the protection functions. In [7], time-domain protection reliability and operation times are evaluated for TLs that connect inverter-based wind power resources to the power system was tested. In [8], a differentiator-smoother filter model to analyze traveling wave (TW)-based protection approaches is implemented in ATP/MODELS language and validated by means of a comparative analysis against the actual time-domain protection relay in which the referred filters are embedded. In [9], a time-domain relay model is presented to emulate time-domain protection behavior. However, no validation process has been presented so far, and although the pilot scheme is considered, communication channel effects have been disregarded.

Although it is well-known that communication channels play a major role for time-domain pilot schemes and differential elements [10], [11], the proper communication channel latency (CCHL) representation in a laboratory environment is usually challenging due to the need for extra long optical fibers to realistically emulate the channel. Thereby, from the best knowledge of the authors regarding works available in the open literature, studies focused on assessing high-speed protection devices in laboratory environments have disregarded the CCHL effects, which can lead to a misinterpretation of what we call here "race of protection functions".

Among the fastest existing TL time-domain protection functions, those based on the theory of TWs and incremental quantities (IQ) stand out, such as: TW-based differential element (TW87); TW- and IQ-based directional elements (TW32 and TD32, respectively); and IQ-based distance element (TD21). The TW32 and TD32 elements analyze polarities in voltage and current TWs and IQs, respectively, which are filtered from the measured signals. These functions are used in a permissive overreaching transfer trip (POTT) scheme to accelerate the trip command issuing. The TD21 is an underreach function that uses IQ data from only one terminal, which can send a direct transfer trip (DTT) to the remote terminal whenever a fault is detected. Finally, the TW87 element compares polarities, amplitudes, and arrival times of current TWs at both TL ends, being included in the DTT logic [1]. Thus, understanding the real tripping times when the CCHL effects are considered is important to properly evaluate the high-speed protection benefits [10].

This paper presents studies on the CCHL effects in the ATP/ATPDraw environment, using the MODELS language to model both analyzed time-domain relay and communication channel. To provide a realistic analysis, the relay model is validated from massive playback tests in a real time-domain device. As a result, a realistic testing platform is obtained, accurately reproducing the relay behavior and CCHL effects.

Eduardo P. A. Ribeiro, Kleber M. Silva, and Amauri G. Martins-Britto are with University of Brasília (UnB), Brazil (email: {eduardopassos, klebermelo, amaurigm}@lapse.unb.br).

F. V. Lopes is with Federal University of Paraíba (UFPB), Brazil (email: {felipelopes}@cear.ufpb.br).

This study was financed in part by the Coordenação de Aperfeiçoamento de Pessoal de Nível Superior - Brazil (CAPES) - Finance Code 001.

Paper submitted to the International Conference on Power Systems Transients (IPST2023) in Thessaloniki, Greece, June 12-15, 2023.

Different ATP fault cases are simulated using a 230 kV/60 Hz test power system modeled with real Brazilian transmission power system data. Moreover, the monitored TL length is varied in order to represent systems with different CCHL values. By assessing the studied time-domain elements, the "race of protection functions" is illustrated considering the CCHL effects. The results demonstrate that the CCHL has a relevant influence on the operating times of pilot schemes and differential elements, in such a way that it must be taken into account whenever detailed tripping time protection studies are required.

## II. Theoretical Review

In this section, the theoretical principles required to understand the CCHL effects and the analyzed time-domain protection schemes are presented.

### A. CCHL Concepts

Fiber-optic channels feature high data transmission capacity, reliability and safety, offering high bandwidth, inherent immunity to electromagnetic interference and exceptional signal-to-noise ratio. These characteristics have made the optical fiber-based channels a widespread medium for modern power system communications [10].

To synchronize data between the two TL terminals, information on the time that a signal takes to travel through the communication channel is required, which is called in this paper CCHL. According to [10], the CCHL is equal to the sum of communication equipment delay and communication path delay. The equipment delay depends on the device features and the communication propagation delay depends directly on the path length and on the electromagnetic wave propagation speed, which according to [10], for fiber-optic channels, is fairly constant and approximately equal to 4.9 $\mu$s per km.

### B. TW87

TW87 scheme triggers the fault identification procedure when a disturbance detection is asserted at both TL terminals. Thereby, it starts a comparison of polarities, amplitudes and arrival time instants of local and remote incident TWs ($i_{TWL}$ and $i_{TWR}$, respectively) [1]–[3], [9], [12]. External faults generate current TWs measured with opposite polarities at the TL terminals, as illustrated in Fig. 1a. On the other hand, internal faults generate TWs measured with the same polarities, as depicted in Fig. 1b.

Besides the polarity comparison, the TWs arrival time indexes at local and remote terminals ($NL_{First}$ and $NR_{First}$, respectively) are analyzed. For internal faults, the absolute difference $P = |NL_{First} - NR_{First}|$ is smaller than the line propagation time ($\tau$) and, for external faults, $P = \tau$ [1], [2], [12]. Furthermore, $\tau$ seconds after the detection of $NL_{First}$ and $NR_{First}$, a search window is applied in order to verify whether there are exit TWs at the opposite TL end ($NL_{Exit}$ and $NR_{Exit}$ for local and remote terminals, respectively). Hence, based on the detected first and exit times, local and

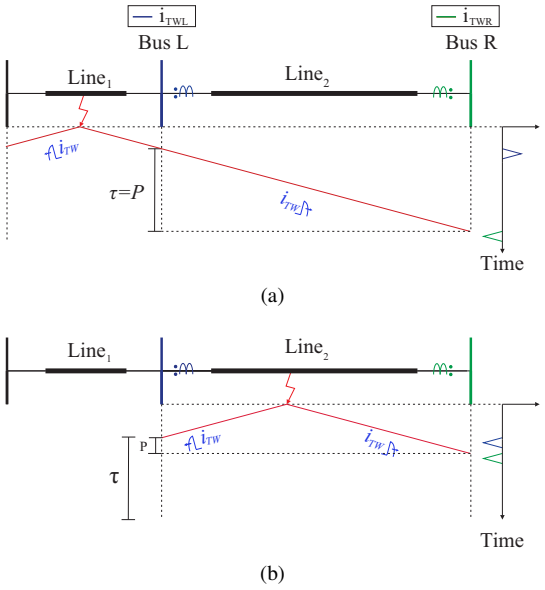


Fig. 1. First $i_{TW}$ measured in the TL terminals for an: (a) external fault on the adjacent TL; and (b) internal fault on the monitored TL.

remote currents ($I_L$ and $I_R$, respectively) are calculated for each phase, as follows:

$$I_{L,K} = C \cdot \sum_{i=-M}^{M} i_{TW,K}[NL_{First} - i \cdot timestep] \ , \quad (1)$$

$$I_{R,K} = C \cdot \sum_{i=-M}^{M} i_{TW,K}[NR_{First} - i \cdot timestep] \ , \quad (2)$$

where $K$ represents each phase, $C = 0.1$ and $M = 20$. Thus, a phase operation quantity given by $I_{Op,K} = I_{L,K} + I_{R,K}$ is calculated to support the phase-segregated tripping decision-making, classifying the faulted phases.

Finally, operating and restraint quantities ($I_{Op}$ and $I_{Res}$, respectively) are calculated, where $I_{Op}$ is taken as the highest computed operating quantity per fault loop ($I_{Op,FL}$), being $I_{Res}$ taken as the maximum restraint quantity calculated at local and remote terminals, which are given by the highest restraint values computed per fault loop ($I_{ResL,FL}$ and $I_{ResR,FL}$, respectively). To obtain the amplitudes of these variables, the following equations are used:

$$I_{Op} = C \cdot \max[I_{OP,FL}] \ , \quad (3)$$

$$I_{Res} = C \cdot \max[I_{ResL,FL}, I_{ResR,FL}] \ , \quad (4)$$

where:

$$I_{Op,FL} = \left| \sum_{i=-M}^{M} i_{TWL,FL}\,[NL_{First} - i] + i_{TWR,FL}\,[NR_{First} - i] \right| \ , \quad (5)$$

$$I_{ResL,FL} = \left| \sum_{i=-M}^{M} i_{TWL,FL}\,[NL_{First} - i] - i_{TWR,FL}\,[NR_{Exit} - i] \right| \ , \quad (6)$$

$$I_{ResR,FL} = \left| \sum_{i=-M}^{M} i_{TWR,FL}\,[NR_{First} - i] - i_{TWL,FL}\,[NL_{Exit} - i] \right| \ . \quad (7)$$

The TW87 protection function counts on additional supervision layers [1], [11], namely: overcurrent supervision; and classical double-ended fault location supervision $m_{87}$, which is in turn applied using the indexes $NL_{First}$ and $NR_{First}$ as follows:

$$m_{87} = \frac{1}{2} \cdot \left[1 + \left(\frac{NL_{First} - NR_{First}}{\tau}\right)\right] . \quad (8)$$

### C. TW32

The TW32 function takes into account the TWs estimated from the voltage signals ($v_{TW}$), which are used in conjunction with $i_{TW}$ in a directional-based analysis to distinguish external from internal faults. This element is used in a POTT scheme. For external faults behind the local bus, as depicted in Fig. 2a, $v_{TWL}$ and $i_{TWL}$ have the same polarities and $v_{TWR}$ and $i_{TWR}$ have opposite polarities. On the other hand, for internal faults, as shown in Fig. 2b, $v_{TW}$ and $i_{TW}$ are measured at both terminals with the same polarities. Thus, if a fault occurs being asserted as a forward indication by the TW32 scheme, it activates a directionality command, sending it to the remote terminal. Hence, in external fault cases, only one terminal sees a forward fault, whereas, for internal faults, both terminals detect a forward fault, confirming that the disturbance occurred within the protected TL. All these commands are exchanged between the TL terminals by means of communication channels, whose CCHL can influence the tripping decision time.

In the TW32 scheme, a TW operation torque $T_{Op,TW} = -v_{TW} \cdot i_{TW}$ is computed, from which operating and restraint energies ($En_{Op,TW}$ and $En_{Res,TW}$, respectively) are calculated using:

$$En_{Op,OV} = \sum_{j=1}^{3} \sum_{k=0}^{49} T_{Op,OV,j}\,[n-k] \ , \quad (9)$$

$$En_{Res,OV} = \sum_{j=1}^{3} \sum_{k=0}^{49} |T_{Op,OV,j}\,[n-k]| \ , \quad (10)$$

where $En_{Op,TW}$ is the sum of fifty $T_{Op,TW}$ samples after the disturbance detection, and $En_{Res,TW}$ is the sum of the absolute values of the fifty $T_{Op,TW}$ samples after a disturbance detection, both computed for the three system phases.

Thus, being $k_{FWD} = 0.75$ and $k_{REV} = 0.5$ slopes applied for forward and reverse fault statements, respectively, if $En_{Op,TW} > k_{FWD} \cdot En_{Res,OV}$ a forward fault is asserted and, on the other hand, if $En_{Op,TW} < -k_{REV} \cdot En_{Res,OV}$ a reverse fault is asserted. Furthermore, some routines are used, as security layers, to enable the above-mentioned statement, among which the following stand out:

- $En_{Op,TW}$ must be higher than a threshold;
- $En_{Op,TW}$ must have the same polarity in each phase under disturbance;
- The pre-fault signals must have the same polarity of $i_{TW}$ and opposite polarity of $v_{TW}$; and
- The condition $\tau > 50$ $\mu$s must be verified and the maximum estimated $i_{TW}$ value times 0.2 is higher than 1% of the current transformer relationship in the monitored terminal.

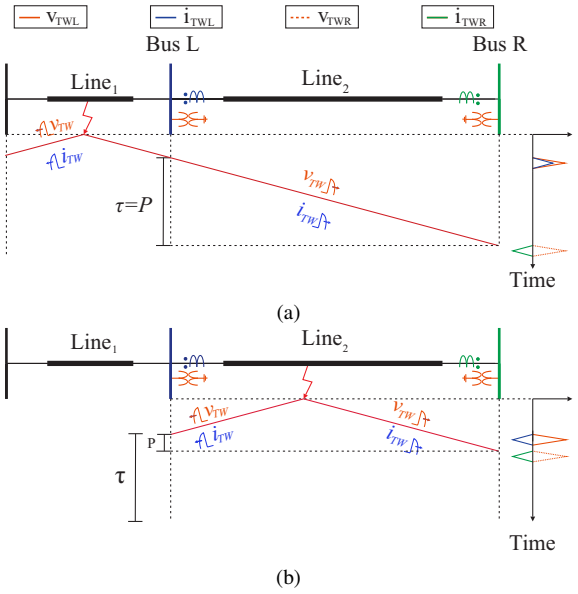


Fig. 2. First $v_{TW}$ and $i_{TW}$ measured in the TL terminals for an: (a) external fault on the adjacent TL; and (b) internal fault on the monitored TL.

### D. TD32

The TD32 protection scheme works with the same directionality patterns of TW32 function, but using IQ voltages and IQs replica currents ($\Delta v$ and $\Delta i_Z$, respectively). POTT scheme also considers the TD32 operation and, when it is confirmed at both TL terminals, a trip command is issued [1], [11]. Considering a TL as an RL circuit, algebraic relationships between $\Delta v$ and $\Delta i_Z$ can be obtained. For protective relays installed on both terminals (L and R) of the TL depicted in Fig. 3a and Fig. 3b, the monitored IQs are related for forward faults as:

$$\Delta v\,(t) = -\,|Z_L| \cdot \underbrace{\left[\frac{R_L}{|Z_L|} \cdot \Delta i\,(t) + \frac{L_L}{|Z_L|} \cdot \frac{d}{dt}\Delta i\,(t)\right]}_{\Delta i_Z(t)}, \quad (11)$$

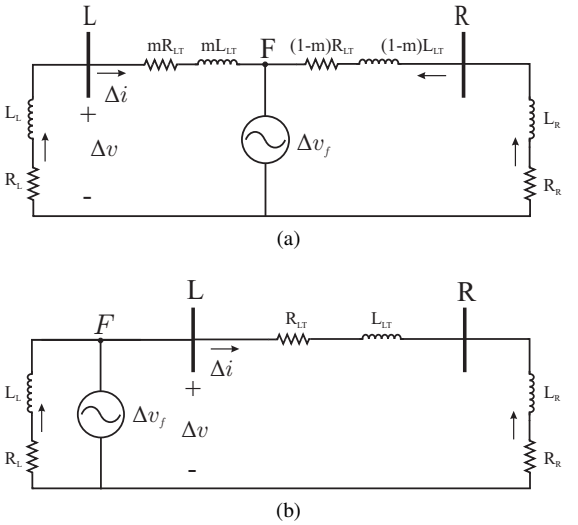


Fig. 3. Simplified pure of fault circuit to a: (a) External fault; e (b) Internal fault in the monitored TL.

and for reverse faults as:

$$\Delta v\left(t\right) = \left|Z_{LT} + Z_R\right| \cdot \underbrace{\left[\frac{R_{LT} + R_R}{\left|Z_{LT} + Z_R\right|} \cdot \Delta i\left(t\right) + \frac{L_{LT} + L_R}{\left|Z_{LT} + Z_R\right|} \cdot \frac{d}{dt}\Delta i\left(t\right)\right]}_{\Delta i_Z(t)} . \tag{12}$$

From the algebraic relationships obtained between $\Delta v$ and $\Delta i_Z$, external and internal faults can be distinguished. Thus, in the TD32 scheme, operation torques, $T_{Op} = -\Delta v \cdot \Delta i_Z$, are computed and adaptive restraint torques for forward and reverse faults ($T_{FWD}$ and $T_{REV}$, respectively), are calculated as follows:

$$T_{FWD}\left(t\right) = TD32ZF \cdot \Delta i_Z^2\left(t\right) \ , \tag{13}$$

$$T_{REV}\left(t\right) = -TD32ZR \cdot \Delta i_Z^2\left(t\right) \ , \tag{14}$$

where $TD32ZF$ and $TD32ZR$ are impedance values adjusted for forward and reverse faults, respectively. Thereafter, the energies $En_{Op}$, $En_{FWD}$ and $En_{REV}$ are computed from the integration of $T_{Op}$, $T_{FWD}$ and $T_{REV}$, respectively. From the analysis of such energies, forward or reverse fault detection logic is asserted if the condition expressed in (15), for forward faults, or (16), for reverse faults, is met [1], [11].

$$En_{Op}\left(t\right) > En_{FWD}\left(t\right) \ , \tag{15}$$

$$En_{Op}\left(t\right) < En_{REV}\left(t\right) \ . \tag{16}$$

### *E. TD21*

The TD21 is also an IQ-based protection function and works as an underreached element. This function is used in the DTT scheme and it only needs a communication channel for sending the trip command to the remote terminal, i.e., it works as a standalone function, so that it issues the trip command to the local terminal without any information from the remote TL end [1]. Thus, although traditional phasor-based TL distance protection functions work by measuring the impedance seen from the terminal and comparing it with the operation characteristics defined from the TL impedance, the TD21 operates based on the analysis of voltage profiles. Hence, according to (17), the voltage at a pre-defined TL point ($m_1$) is estimated as:

$$v_{m_1}\left(t\right) = v\left(t\right) - m_1 \cdot \left|Z_{LT1}\right| \cdot i_Z\left(t\right) \ , \tag{17}$$

being its IQ absolute value $\left|\Delta v_{m_1}\left(t\right)\right|$ used as an operation quantity $v_{Op}\left(t\right)$ in the TD21 protection scheme [2].

The highest possible instantaneous voltage variation in $m_1$ during a disturbance is $-v_{m_1}\left(t\right)$, i.e., $\left|v_{m_1}\left(t\right)\right| = \left|\Delta v_{m_1}\left(t\right)\right|$. From this premise, the TD21 restraint quantity $v_{Res}\left(t\right)$ illustrated in Fig. 4 is calculated, being given by the highest value between: $v_{m_1}\left(t\right)$ delayed of a fundamental cycle, $v_{m_1}\left(t-T\right)$; $dt$ samples around $v_{m_1}\left(t-T\right)$, $v_{m_1}\left(t-T+dt\right)$ and $v_{m_1}\left(t-T-dt\right)$; and a voltage lower safety threshold.

Considering solid faults, i.e., fault resistance equal to zero ($R_f = 0\ \Omega$), if a fault occurs at $m_1$, as illustrated in Fig. 5a, $v_{Op} \approx v_{Res}$. On the other hand, if a fault occurs behind $m_1$, as shown in Fig. 5b, $v_{Op} > v_{Res}$. Finally, if a fault occurs beyond $m_1$, as depicted in Fig. 5c, $v_{Op} < v_{Res}$. Thus, when a fault occurs behind $m_1$, the voltage difference between $v_{Op} - v_{Res}$ is integrated and, if it is larger than a security margin, a trip command is issued.

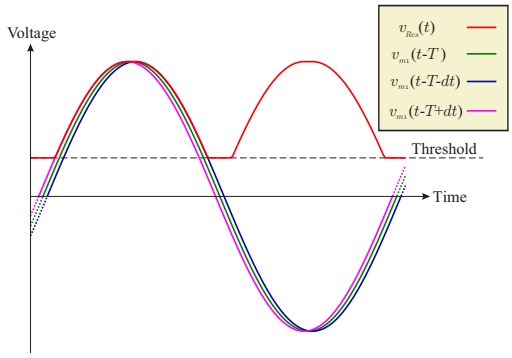


Fig. 4. TD21 $v_{Res}$ calculation [2].

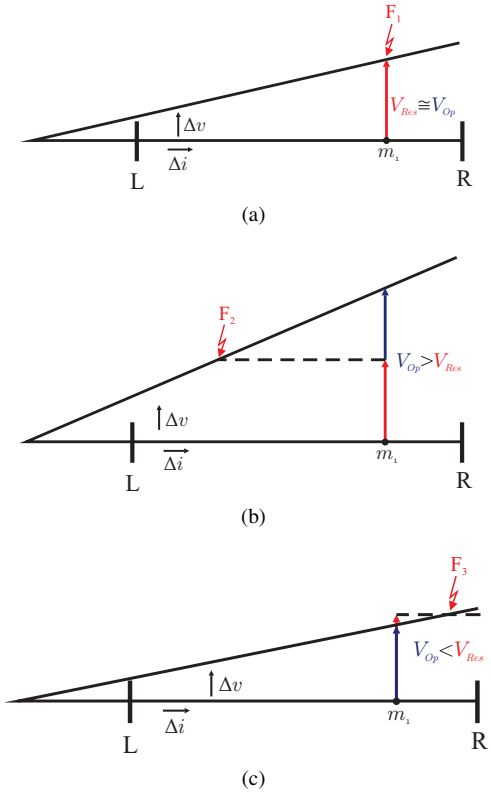


Fig. 5. $v_{Op}$ *vs* $v_{Res}$ profile: (a) Fault located at $m_1$; (b) Fault located before $m_1$; e (c) Fault located after $m_1$ [1], [13].

## III. Validation Description

In this section, the implemented relay model and its validation case studies are explained. Since this paper is mainly focused on the analysis of CCHL effects on the described time-domain functions rather than on the detailed description of the relay model implementation in the ATP/ATPDraw environment, details on the internal functional blocks of the relay model and on the MODELS codes used to implement the analyzed time-domain functions are not presented. Even so, the main aspects related to the relay model implementation, simulation cases used in the validation procedures as well as the results obtained from a comparative

analysis between the implemented model and the actual time-domain relay are discussed and sufficiently detailed to allow a proper understanding about the final results.

### A. Test System and Studied Fault Scenarios

As mentioned earlier, in order to include the CCHL effects without the need for having long optical fibers in a laboratory environment, the analyzed time-domain relay was developed using the ATP/ATPDraw platform by means of the MODELS language. The TW87, TW32, TD32 and TD21 protection schemes described in the previous section were taken into account, being initially validated through case studies in the 230 kV/60 Hz test power system depicted in Fig. 6. A total of 162 faults on the monitored line were simulated, varying: the fault type (AG and AB faults); the fault location ($m$) from 0.1 p.u to 0.9 p.u with steps of 0.1 p.u.; the $R_f$ from 0 Ω (solid fault) to 50 Ω with steps of 25 Ω; and the fault inception angle ($\theta$) from 0° from 90° with steps of 45° (considering a sine reference). The test power system was modeled with real data from Brazilian lines, being the power grids surrounding the line represented by two Thevenin equivalents placed at the system terminations, which are connected to buses L and R by means of 100 km TLs. The protected line is 200 km long, and it connects the bus L to bus R, i.e., the protected line has adjacent TLs at both ends, as shown in Fig. 6. Also, coupling capacitor voltage transformers (CCVTs) and current transformers (CTs) were intentionally modeled as ideal apparatus, since the focus here is not to evaluate the impact of their transient response, but rather, the CCHL effects.

The ATP/ATPDraw simulations were run using a 1 us time step, with a maximum simulation time of 0.08 s. Since the relay model functions require data windowing procedures, the first power cycle in the obtained signals is disregarded, which could be compared to the actual relay arming logic [1]. In summary, such an arming logic requires some stable quantities to be measured before the relay protections are activated. Then, soon after the relay is armed, all described functions are enabled to trip the line if an internal fault is detected.

### B. ATP/ATPDraw Relay Model Validation

The ATP/MODELS time-domain protection relay model depicted in Fig. 6 was developed in two steps: 1) The signals processing algorithms used to extract the TW-based and IQ-based quantities from the measured fault-generated signals were studied and developed in the first step; and 2) The protection elements based on the analysis of quantities obtained from the signals processing techniques were developed in the second step. In this step, inputs and outputs of each protection function were thoroughly evaluated in order to approximate the ATP/ATPDraw relay model as much as possible to the actual relay response. To do so, the references [1]–[4], [11], [13] were used as guidelines to implement the ATP/MODELS relay model.

In order to proper validate the ATP/MODELS relay model, including the signal processing tools and the protection functions, voltage and current signals measured at buses L and R were recorded in all simulation cases, being then applied to the actual time-domain relay via its own playback testing

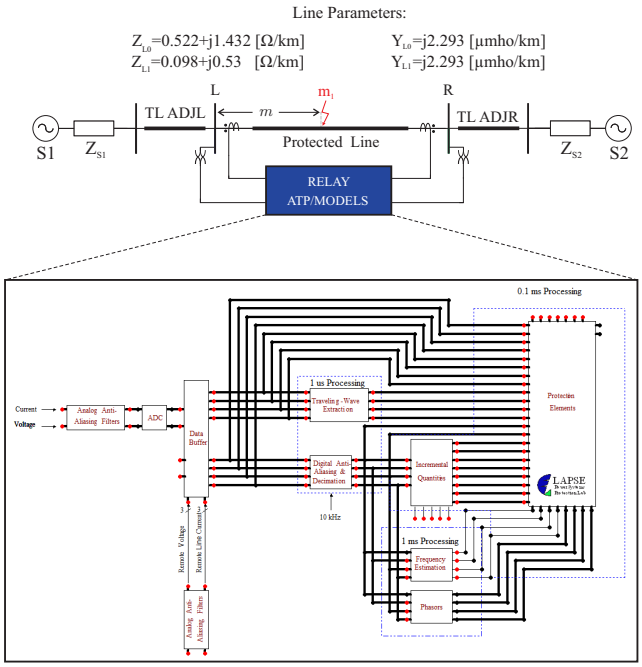


Fig. 6. Test power system.

feature, which is described in detail in [1]. As the first obtained results, the signals processing validation is illustrated in Fig. 7, considering records obtained from a single fault case related to an AG solid-to-ground fault located at 0.2 p.u. from bus L, and with inception angle $\theta$ equal to 90°. In Fig. 7a, the TW-based quantities validation is presented according to [8], and in Fig. 7b the IQ-based validation is presented. The obtained results reveal that the signals calculated from the ATP/MODELS relay model fit very well those obtained from the actual time-domain relay. Indeed, comparing both simulated model and real device responses, it can be seen that the curves are visually overlapped, which reveals that only negligible discrepancies exist. Therefore, one can conclude that the modeled relay properly emulates the signals processing functions embedded in the real device, allowing to obtain reliable representations of both TW and IQ quantities.

Finally, as the second part of the ATP/MODELS relay model validation, the results obtained from the 162 simulated fault cases for each function were collected in the form of tripping times from playback tests in the real relay. The collected results were then compared against the tripping times obtained from the developed ATP/MODELS relay model.

To provide a didactic comparison between the tripping times obtained from the real and simulated relays, probability density curves are used to represent the distribution pattern of the obtained tripping times. In other words, these probability density curves represent the number of cases per tripping times verified in the analyzed case studies, such that they can visually demonstrate the overall behavior of both real and simulated relays from the perspective of the number of cases for which a specific tripping time was verified. The obtained results are shown in Fig. 8. The results reveal that the modeled TW-based protection functions presented a very

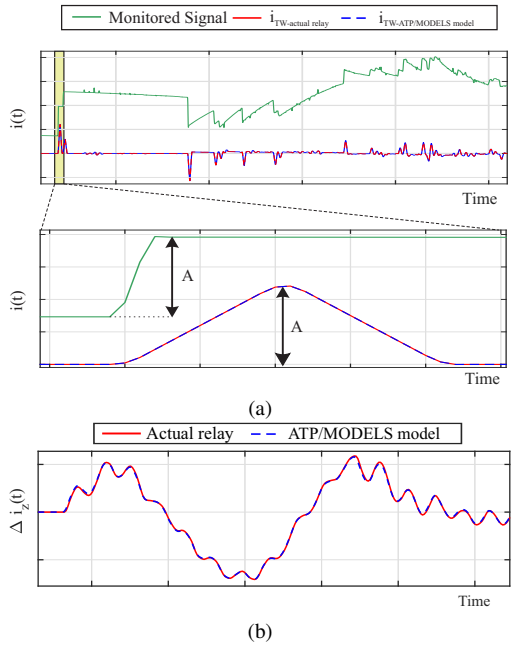


Fig. 7. Sinal processing validation: (a) TW signals [8]; (b) IQ signals.

good concordance in relation to the relay response, except for slight deviations found in the TW32 function for tripping times within the range of values until 0.4 ms. Similarly, TD functions also showed to be satisfactorily adherent to the real relay response, presenting only slight differences in the verified tripping times. Regarding the TD32 function, the deviations were verified mostly for tripping times around 2.5 ms. On the other hand, considering the TD21 function, the deviations showed up mainly for tripping times in between 7.5 and 10 ms. It is worth mentioning that these deviations are not considered critical, since they come from discrepancies of only one to two samples of slower of faster responses. Indeed, in the authors' opinion, it consists in acceptable deviations. Therefore, one can consider that the developed ATP/MODELS routines can reliably be used to carry out studies on the CCHL effects from the perspective of protection tripping times.

## IV. Obtained Results and Discussions

On applying time-domain-based protection functions, a question may arise: which function is faster when the CCHL is taken into account? Thus, in this section, the results of what is called "race of protection functions" are analyzed. To do so, a new set of 648 fault cases were simulated in the power system presented in Fig. 6, using the parameters shown in Table I. In these cases, the CCHL influence over the tripping times of the developed ATP/MODELS relay model is assessed when different TL lengths are considered.

### A. CCHL Influence

Fig. 9 depicts the obtained results per protective scheme studied in this paper, allowing to verify the influence of the CCHL over different TL lengths. In Fig. 9a, it is illustrated that the CCHL regards to a large part of the tripping time of the TW87 function. Fig. 9b shows that the CCHL is a relevant factor over the POTT scheme. Fig. 9c demonstrates that using

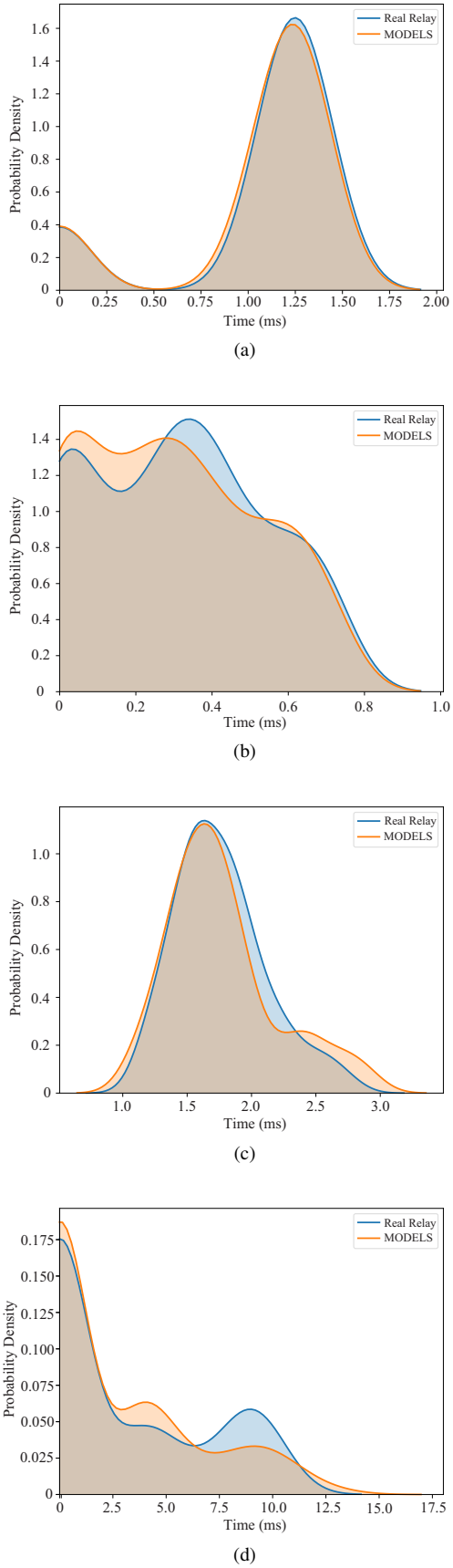


Fig. 8. Density probability from the obtained results for: (a) Relay-TW87 $vs$ ATP-TW87; (b) Relay-TW32 $vs$ ATP-TW32; (c) Relay-TD32 $vs$ ATP-TD32; and (d) Relay-TD21 $vs$ ATP-TD21.

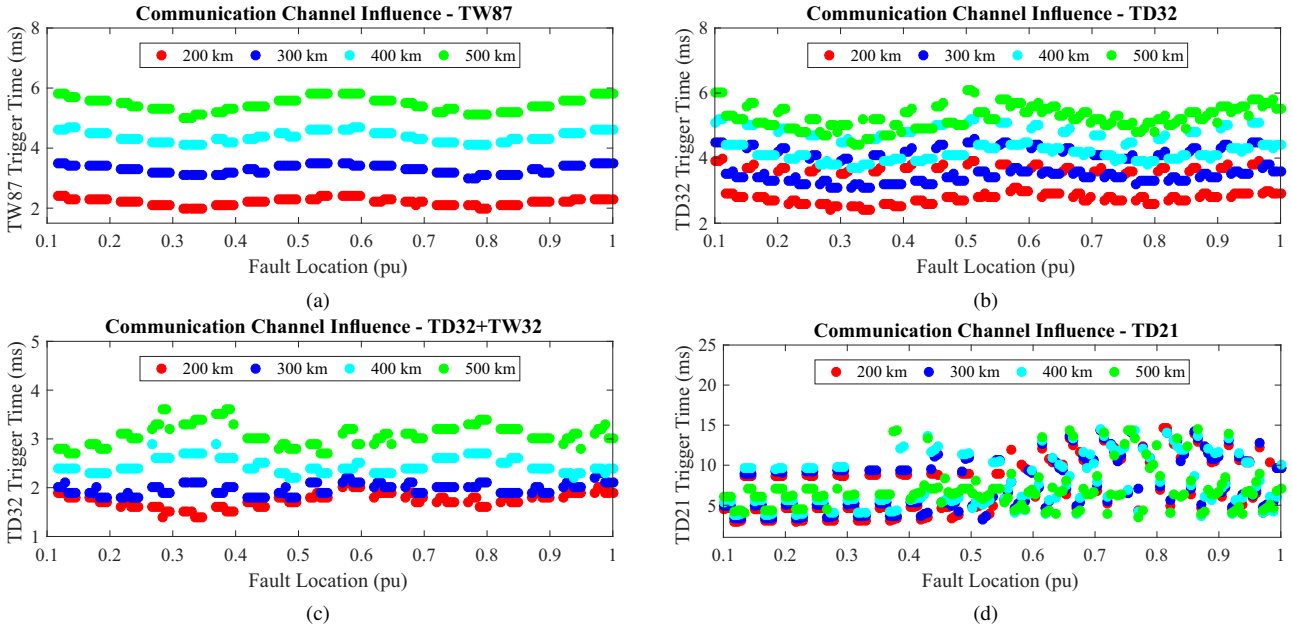


Fig. 9. CCHL Influence per protective scheme: (a) TW87+DTT; (b) TD32+POTT; (c) TD32+TW32+POTT; and (d) TD21+DTT.

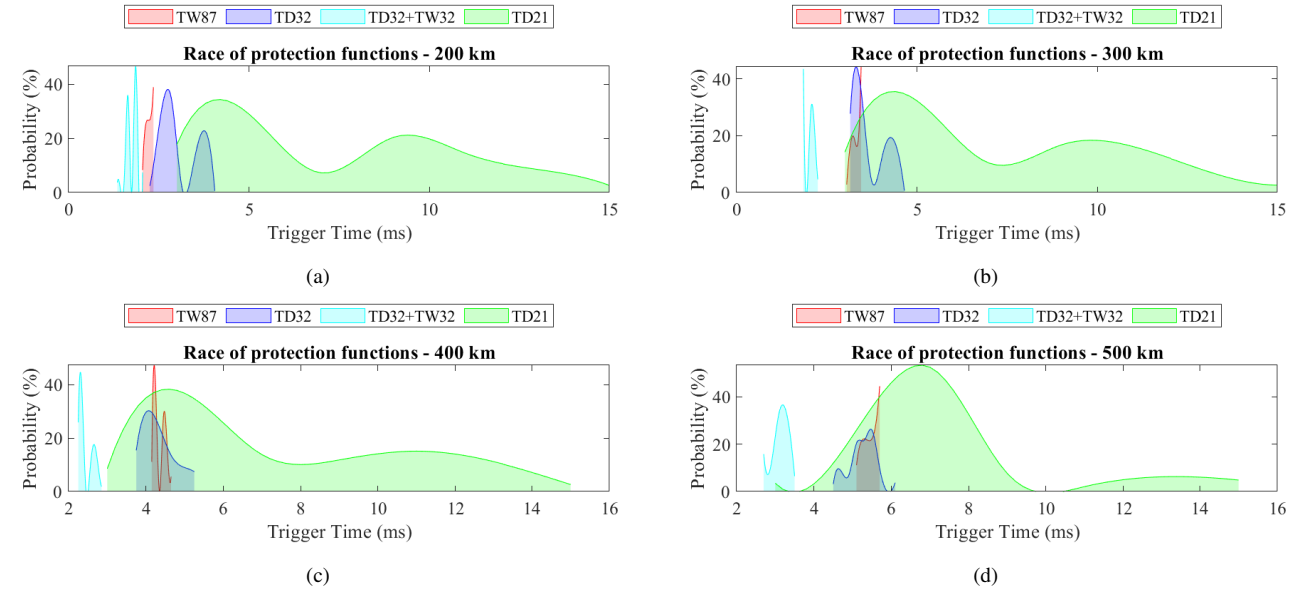


Fig. 10. Race of time-domain protection functions for different TL lengths ($l$): (a) $l = 200$ km; (b) $l = 300$ km; (c) $l = 400$ km; and (d) $l = 500$ km.

TABLE I
PARAMETERS USED IN THE ASSESSMENT OF CCHL EFFECTS.

| *TL length (km)* | **Fault type** | $m$ (p.u.) | $R_f$ ($\Omega$) | $\theta$ (°) |
|---|---|---|---|---|
| 200 | AG | 0.1; 0.2; 0.3; | 0 | 0 |
| 300 | | 0.4; 0.5; | 25 | 45 |
| 400 | BG | 0.6; 0.7; | 50 | 90 |
| 500 | | 0.8; 0.9 | | |

the TW32 protection scheme to speed up the TD32 tripping command brings more benefits for 300 km, 400 km and 500 km lengths. Finally, in Fig. 9d it is possible to conclude that the CCHL influence over TD21 trigger time is not a major factor to define its operating time, which was already expected since it consists in a non-unit protection which requires only single-ended data.

### *B. Race of Time-Domain Protection Functions*

Fig. 10 depicts the probability distribution related to the tripping times verified for each evaluated TL length, forming which the authors call as "race of time-domain protection functions". This figure allows to identify the fastest protection functions when the TL length is varied, thus varying the CCHL influence. From Fig. 10a, it is noticed that the TW87, TD32 and TD32+TW32 protective schemes remain being the fastest ones, except in some cases in which TD21 gets shorter tripping times. Through the analysis of the Fig. 10b, one can

see that the shortest tripping times are clearly obtained when the TW32 is used to speed up the TD32 protective scheme. Also, one can notice that, in some cases, TD21 results in fault clearance times similar to those obtained in the TW87 and TD32 schemes. In Fig. 10c it can be confirmed that, as TL length increases, the TD21 can become faster than the other functions, tending to be slower than the TD32+TW32 scheme in the most critical fault cases. In this context, it is important to mention that this result is consistent, because the TD32 is used in the TD21 tripping logic. Thus, the results demonstrate that the TD32 did not delay the TD21 tripping time in the evaluated cases. As a last analysis, from Fig. 10d, it can be concluded that the combination of TD32 and TW32 functions consist in the fastest protective scheme, irrespective of the transmission line length. Indeed, for shorter lines, TD32+TW32 and TW87 tend to be the fastest ones, in this sequence. However, as the TL gets longer, additional delays affect TW87 and TD32, leading the TD32+TW32 and TD21 to "win the race". It is worthy noting that the TW32 accelerates the POTT scheme, whose trip issuance is based on the TD32. Thus, although the POTT scheme requires the communication channel, by combining the TW32 with the TD32, a very quick fault directionality detection is performed, and the trip decision via TD32 is required to be obtained only locally, which compensates the CCHL effect.

## V. Conclusions

In this paper, the communication channel latency (called here CCHL) influence on time-domain protection schemes is studied, in order to verify which functions among those embedded into a real time-domain relay are the fastest ones when different CCHL levels are considered. Such type of study is difficult to carry out in laboratory environments, because very long fiber-optic communication channels are necessary. Therefore, an ATP/ATPDraw time-domain relay model was developed and case studies of faults on four different TL with lengths equal to 200 km, 300 km, 400 km and 500 km were conducted. Since the CCHL depends also on the transmission line, a "race of time-domain protection functions" could be demonstrated for the studied scenarios.

From the obtained results, it is demonstrated that the combination of TD32 and TW32 functions result in the fastest time-domain scheme for all evaluated cases. When considering the CCHL latency, the operating times of the TW87 get slower as the TL length increases, being the TW87 the second fastest function, according to the simulated cases considering lengths of 200 km. However, the TW87 "passed in the finish line or the race" in third place or even in the last place in some cases where TL lengths of 400 km and 500 km were considered. Finally, it can be observed that the TD21 operating times were little influenced when the CCHL was considered in the DTT scheme. Such a function became faster in relation to other functions as the TL length was increased, being the second fastest function in some cases for the TL with length equal to 500 km. Therefore, these results reveal the importance of considering the CCHL during studies on the operation speed of time-domain functions, whose tripping times can become somewhat unrealistic when the CCHL effects are disregarded. Finally, the authors intend to demonstrate the importance of considering communication channel models in protection studies, specially when the main focus is on the time-domain tripping times.

## References


[1] *Ultra-High-Speed Transmission Line Relay Traveling-Wave Fault Locator High-Resolution Event Recorder*, Schweitzer Engineering Laboratories, 2019. [Online]. Available: https://selinc.com/products/T400L/

[2] E. O. Schweitzer, B. Kasztenny, and M. V. Mynam, "Performance of time-domain line protection elements on real-world faults," in *2016 69th Annual Conference for Protective Relay Engineers (CPRE)*. IEEE, 2016, pp. 1–17.

[3] E. O. Schweitzer, B. Kasztenny, A. Guzmán, V. Skendzic, and M. V. Mynam, "Speed of line protection-can we break free of phasor limitations?" in *2015 68th Annual Conference for Protective Relay Engineers*. IEEE, 2015, pp. 448–461.

[4] R. Abboud and D. Dolezilek, "Time-domain technology–benefits to protection, control, and monitoring of power systems," in *International Conference and exibition-relay protection and automation for electric power systems*, 2017, p. 16.

[5] E. P. A. Ribeiro, K. M. e Silva, F. V. Lopes, and A. Martins-Britto, "Time-domain-based relay model to assess line protection nearby HVDC systems," in *2021 Workshop on Communication Networks and Power Systems (WCNPS)*. IEEE, 2021, pp. 1–6.

[6] F. V. Lopes, C. M. Ribeiro, J. P. G. Ribeiro, and E. J. S. Leite Jr, "Performance evaluation of the travelling wave-based differential protection when applied on hybrid transmission lines," *The Journal of Engineering*, vol. 2018, no. 15, pp. 1114–1119, 2018.

[7] J. S. Costa, R. T. Toledo, L. A. Gama, T. R. Honorato, F. V. Lopes, P. S. Pereira, G. S. Salge, and M. J. Davi, "Phasor-based and time-domain transmission line protection considering wind power integration," *15th International Conference on Developments in Power System Protection (DPSP 2020)*, 2020.

[8] E. P. A. Ribeiro, F. V. Lopes, J. P. G. Ribeiro, and E. J. Leite, "ATP/MODELS differentiator-smoother filter model validated using actual time-domain relay," in *2018 Workshop on Communication Networks and Power Systems (WCNPS)*. IEEE, 2018, pp. 1–4.

[9] J. P. G. Ribeiro and F. V. Lopes, "Modelling and simulation of a time-domain line protection relay," *The Journal of Engineering*, vol. 2018, no. 15, pp. 861–865, 2018.

[10] H. J. A. Ferrer and E. O. Schweitzer, *Modern solutions for protection, control, and monitoring of electric power systems*. Schweitzer Engineering Laboratories Pullman, Washington, DC, USA, 2010.

[11] N. Metzger, B. Carstens, and F. Heleniak, "Practical experience with ultra-high-speed line protective relays"," in *22nd Annual Georgia Tech Fault and Disturbance Analysis Conference*, 2018.

[12] F. V. Lopes, J. P. G. Ribeiro, E. J. Leite, and K. M. Silva, "Parametric analysis of the travelling wave-based differential protection tw87," *The Journal of Engineering*, vol. 2018, no. 15, pp. 1297–1302, 2018.

[13] B. Kasztenny, A. Guzmán, N. Fischer, M. V. Mynam, and D. Taylor, "Practical setting considerations for protective relays that use incremental quantities and traveling waves," in *proceedings of the 43rd Annual Western Protective Relay Conference, Spokane, WA*, 2016.